Voltage-driven displacement of magnetic vortex cores

M. Ghidini[1,2,3,*], R. Pellicelli[4], R. Mansell[5,#], D. Pesquera[3], B. Nair[3], X. Moya[3], S. Farokhipoor[3], F. Maccherozzi[2], C. H. W. Barnes[5], R. P. Cowburn[5], S. S. Dhesi[2], N. D. Mathur[3,†]

[1] Department of Mathematics, Physics and Computer Science, University of Parma, 43124 Parma, Italy.

[2] Diamond Light Source, Chilton, Didcot, Oxfordshire, OX11 0DE, UK.

[3] Department of Materials Science, University of Cambridge, Cambridge, CB3 0FS, UK.

[4] Istituto d'Istruzione Superiore A. Zanelli, 42123 Reggio Emilia, Italy.

[5] Cavendish Laboratory, University of Cambridge, CB3 0HE, UK.

Now at NanoSpin, Department of Applied Physics, Aalto University, FI-00076 Aalto, Finland

* massimo.ghidini@unipr.it

† ndm12@cam.ac.uk

Magnetic vortex cores in polycrystalline Ni discs underwent non-volatile displacements due to voltage-driven ferroelectric domain switching in single-crystal $BaTiO_3$ (BTO). This behaviour was observed using photoemission electron microscopy (PEEM) to image both the ferromagnetism and ferroelectricity, while varying in-plane sample orientation. The resulting vector maps of disc magnetization match well with micromagnetic simulations, which show that the vortex core is translated by the transit of a ferroelectric domain wall, and thus the inhomogeneous strain with which it is associated. The non-volatility is attributed to pinning inside the discs. Voltage-driven displacement of magnetic vortex cores is novel, and opens the way for studying voltage-driven vortex dynamics.

Introduction

Magnetic vortices and skyrmions are topological structures that currently attract huge interest because their nanoscale dimensions [1,2] and inherent stability [3-5] render them suitable for storing and carrying information [6,7]. Moreover, they can be manipulated by static [8] and variable [9] magnetic fields, electric currents [10,11], voltage [12-16] and strain [17]. Magnetic vortices can display four stable states because the core can be magnetized up or down (vortex polarity), and the surrounding in-plane magnetization can curl clockwise or anticlockwise (vortex chirality). Given that polarity and chirality can be independently switched by both magnetic fields and electric currents [8-10,18], researchers have been stimulated to pursue the prospect of magnetic media with two bits per element [19,20].

Magnetic data storage devices would be more energy efficient if data were written using electric fields instead of electric currents or magnetic fields. This technological goal forms a core aspect of the large volume of research into magnetoelectric effects [21], where voltage-controlled magnetic order has been demonstrated in different types of materials. Juxtaposing a magnetic film with another material (typically, but not exclusively a ferroelectric) can result in large room-temperature magnetoelectric effects that are mediated by strain [22-26], charge [27] or exchange bias [28-30]. These magnetoelectric effects may be identified in the magnetic film via changes of magnetization [22,28,31], anisotropy [32,33], coercivity [34] and magnetic domain wall motion [35]. Moreover, the strategy of juxtaposition can achieve magnetoelectric control of magnetic vortices [13-16] and skyrmions [36].

Vortex core displacements have been driven by magnetic fields [9,37] and electrical currents [10], permitting core gyration and core polarity switching, but the voltage-driven motion of a vortex core has been hitherto studied only theoretically [38]. Here we report the first experimental demonstration of this phenomenon by studying polycrystalline Ni discs (diameter 2 μm, thickness 25 nm) that were grown on a ferroelectric substrate of BTO. By imaging the magnetic structure of the discs as well as the surrounding ferroelectric domains, we find that vortex cores are displaced after ferroelectric domain switching has taken place ($a \rightarrow c \rightarrow a$). Corroborative micromagnetic simulations required just 60% of the 10^{-2} uniaxial strain associated with this switching. These simulations show that the vortex core tracks the passing *a*-*c* domain wall, implying that the vortex

core is translated by the inhomogeneous strain associated with the ferroelectric domain wall. The vortex core does not return to its central starting position due to pinning inside the magnetic disc. Our findings complement the studies of vortex core displacement using magnetic fields [9,37] and electrical currents [10], and should stimulate further work on the magnetoelectric control of magnetic vortices.

Experimental methods

We used electron-beam-assisted evaporation to deposit Ni discs of thickness 25 nm and diameter 2 μm on electroded substrates of 0.5-mm thick BTO in the pseudo-cubic (001) orientation [Fig. 1]. The discs were capped with 3 nm of Cu, and formed 10×10 arrays with nearest-neighbour centre-to-centre separations of 6 μm. All fabrication details are given in [13], where the samples differ because the Ni discs are 1 μm in diameter (such that vortex states are magnetoelectrically annihilated rather than modified as they are here). Note that vortices are known to form in nominally unstrained discs of both sizes [39].

PEEM with contrast from x-ray magnetic circular dichroism (XMCD) was to image used to image the magnetic order in our Ni discs, PEEM with contrast from x-ray linear dichroism (XLD) was used to image the surrounding ferroelectric domains in BTO, and PEEM with contrast from x-ray absorption (XAS) was used to image topographical/chemical contrast. The PEEM probe depth was ~7 nm and the lateral resolution was typically ~50 nm. We show either averaged PEEM images, or magnetic vector maps that are derived from averaged XMCD-PEEM images obtained for two orthogonal sample orientations. All details are exactly as specified in [13].

Micromagnetic simulations performed using MuMax3 [40] are detailed in [13]. The resulting vector maps average the magnetization in the top 5 nm, which is similar to the ~7 nm PEEM probe depth. We have neglected the relatively small cubic magnetocrystalline anisotropy of Ni (K_c = -5 kJ m^{-3}) [22] because it averages out in our polycrystalline discs where the grains are small (a lateral size of ~100 nm was recorded for similar films [22]). Simulations that discretized a disc into randomly oriented grains of this lateral size yielded similar results, and so our assumption of a continuous medium is reasonable.

Experimental results

The XAS-PEEM image in Fig. 1(b) confirms the presence of the Ni discs, three of which are numbered for later. Fig. 2 shows composite images of the sample in its virgin state, as the in-plane sample orientation was varied from 0° [Fig. 2(a)] to 45° [Fig. 2(b)] to 90° [Fig. 2(c)]. The XMCD-PEEM data for the discs reveals magnetic inhomogeneity in all but three discs, which are uniformly dark in each image. The XLD-PEEM data for the intervening BTO reveals two types of ferroelectric domain [Fig. 2(a)], which are not resolved after rotating by 45° [Fig. 2(b)], and which reappear with inverted contrast after rotating by 90° [Fig. 2(c)]. The ferroelectric domains are therefore identified as a_1-a_2 domains, with *c*-axis polarizations that alternate between *x* and *y*, as shown via the blue schematics that depict tetragonal unit cells.

The composite image in Fig. 2(c), which we repeat in Fig. 3(a), is modified by the application of 150 V across the BTO substrate, such that the a_1-a_2 domains are annihilated in favour of a single *c*-domain [Fig. 3(b)]. This 90° ferroelectric domain switching imparts uniaxial compressive stress to all Ni discs along either *x* or *y*, according to the orientation of the annihilated *a* domain. The switching aligns magnetic domain walls with the local compression, as expected given that domains in negative-magnetostriction Ni should be magnetized along this direction. Magnetic domain walls that were present before applying the voltage [Fig. 3(a)] are thus rotated by 90° by the ferroelectric domain switching [Fig. 3(b)].

Vector maps of magnetization were obtained for discs 1-3 before, during and after applying the 150 V (Fig. 4). Initially at 0 V, discs 1 and 2 present vortex states that are anisotropic, such that they contain the domain walls discussed earlier [13]. These domain walls are Néel walls given that the magnitude of the XMCD asymmetry remains fairly constant across them, i.e. the magnetization remains in-plane, as expected for a magnetic material whose thickness is just 25 nm. The vortex anisotropy arises as a consequence of the tensile growth strain that is associated with the underlying *a* domain in the BTO substrate [41]. The anisotropic vortex state is dominated by the presence of two large regions that possess a net magnetization along the direction of compressive strain, even though these two regions are inhomogeneously magnetized to yield curling on each side of the intervening Néel walls that widen on approaching the disc edge. Note that this

configuration should not be mistaken for a Bloch line, which lies between homogeneous Néel walls separating homogenous magnetic domains [42].

The application of 150 V rotates the average direction of magnetization by 90°, enhances the anisotropy of the magnetization distribution, and creates in each domain wall multiple chiral discontinuities (vortex/antivortex cores). The return to 0 V restores a magnetization distribution that is reminiscent of the initial state. However, the multiple vortex cores that were created at 150 V are seen to persist and be displaced off-centre. This complexity (and the complexity that we will now describe for Disc 3) is possible because our discs are large enough to support metastable states.

Disc 3 behaves differently [Fig. 4(g-i)]. It formed a single domain at 0 V, despite exceeding the critical diameter, which is 400 nm for a Ni disc of this thickness [39]. This is because the single-domain state was stablized by tensile growth strain from the BTO substrate, as seen for 1 μm-diameter discs of Ni, whose magnetization lay perpendicular to the underlying ferroelectric polarization as expected [41]. Here, the magnetization lay at ~45° to the underlying ferroelectric polarization, perhaps because the relatively small underlying *a* domain experienced compressive strain from ferroelectric domains elsewhere. The application of 150 V caused the disc to develop two anisotropic vortices, with the preferred magnetization along *x*. On returning to 0 V, vortex cores are created (annihilated) along the upper (lower) Néel wall, whose position is barely modified.

Modelling

The lowest energy state for unstrained Ni discs of our size would be an isotropic vortex [39], as we have confirmed for ourselves, but this was not observed here because of the growth strain. Assuming this strain to be $\varepsilon_y = 2\times10^{-3}$ resulted in an anisotropic vortex [Fig. 5(a)] that matches well the initial state of disc 1 [Fig. 4(a)] and captures the curling and wall widening discussed above. We previously found that BTO produces exactly this growth strain in Ni discs of the same thickness and half the diameter [13], resulting in an anisotropy constant $K = -\frac{3}{2}E\varepsilon_y\lambda = -10$ kJ m^{-3} that has the correct order of magnitude for Ni films on BTO [22].

The $a \rightarrow c$ switching at 150 V [Fig. 3(b)] is represented by switching the tensile strain of $\varepsilon_y = 2\times10^{-3}$ to a compressive strain of $\varepsilon_y = -4\times10^{-3}$ (K = 20 kJ m^{-3}). This produces an anisotropic vortex [Fig. 5(b)] that corresponds to the state of disc 1 at 150 V [Fig. 4(b)]. In agreement with experiment, the vortex is not annihilated, and its preferred magnetization direction is rotated by 90°. Moreover, the multiple vortex/antivortex cores that we observed arise in our model [Fig. 5(c)] by accessing a state that is just 0.2% higher in energy than the ground state with a single vortex core [Fig. 5(b)]. The observation of multiple vortex/antivortex cores is therefore energetically reasonable. Note that the Néel wall containing these cores [Fig. 5c,f] should not be confused with a cross-tie wall, in which the energy cost of a 180° domain wall is avoided by the presence of 90° domains.

On returning to 0 V, imposing the *y*-axis strain associated with $c \rightarrow a$ switching would recover the initial vortex state in our simulations, and the observed displacement of the core cannot be achieved by varying the magnitude of this homogeneous strain (which only modifies the degree of anisotropy [13]). We will therefore proceed to understand the observed core displacement by considering the inhomogeneous strain associated with the passage of an *a*-*c* wall during the switching process (Fig. 6), neglecting spin precession effects because ferroelectric domain motion is slower than spin dynamics. Regions of the disc that overlie the *a* domain experience the tensile growth strain along *y*, whereas regions of the disc that overlie the *c* domain experience the compressive strain along *y*. Motion of the negligibly thick wall displaces the vortex core, which is repelled by the strain (and resulting magnetic anisotropy) gradient, thus reducing the exchange energy. The vortex core displacement is reversible, except for the final step [Fig. 6(j→k)] that recovers the state we simulated with $\varepsilon_y = 2\times10^{-3}$ [Fig. 5(a)]. Similar simulations of the multivortex state reveal that the cores are initially displaced and compressed [Fig. 7(a→g)] until they coalesce into a single core [Fig. 7(g→h)], which then [Fig. 7(i→k)] mimics the single core that is described in Fig. 6.

The non-volatile vortex core displacement that we observed for discs 1-2 [Fig. 4] can be understood by considering both the inhomogeneous strain associated with the ferroelectric domain wall, and pinning associated with the ferromagnetic domain walls in the anisotropic vortex state. In the absence of pinning, the passage of the ferroelectric domain wall would recover the ground

state with a vortex core at the disc centre. However, we may infer that the wall is pinned by defects, such that the vortex core does not return to the centre [Fig. 6(j→k)].

The magnitudes of the strains that reproduce our experimental data are similar to the strains that created and annihilated vortices in 1 μm-diameter discs of Ni on BTO [13], and yet here the vortices are not annihilated. Replacing the tensile growth strain of 2×10^{-3} with the compressive strain of -4×10^{-3} implies that the $a \rightarrow c$ switching produced a compressive strain of -6×10^{-3}, which is 60% of the 10^{-2} uniaxial strain calculated from the BTO lattice parameters for 90° ferroelectric domain switching.

In summary, we have used XMCD-PEEM to study anisotropic magnetic vortices in 25 nm-thick Ni discs of diameter 2 μm, and we have used XLD-PEEM to study the surrounding BTO substrate. Voltage-driven ferroelectric domain switching served to modify—but not annihilate—the vortices, whose cores underwent non-volatile displacement. Using micromagnetic simulations, we attribute this displacement to the inhomogeneous strain associated with the transit of a ferroelectric domain wall, and we attribute the non-volatility to the pinning of the ferromagnetic walls in the anisotropic vortices. Our demonstration of voltage-driven core motion is novel, and could pave the way for time-resolved studies of voltage-driven core dynamics. Such studies would require epitaxial discs of excellent crystal quality, and fast, repeatable pulses of inhomogeneous strain.

Acknowledgments

We acknowledge Diamond Light Source for time on I06 under proposal SI11843. X.M. is grateful for support from the Royal Society. B.N. is grateful for the support from Gates Cambridge, the Winton Programme for the Physics of Sustainability and Trinity College (Cambridge). D.P. acknowledges Agència de Gestió d'Ajuts Universitaris i de Recerca (AGAUR) from the Catalan government for Beatriu de Pinós postdoctoral fellowship (2014 BP-A 00079).

References

[1] Wachowiak A, Wiebe J, Bode M, Pietzsch O, Morgenstern M and Wiesendanger R 2002 *Science* **298** 577

[2] Yu X Z, Onose Y, Kanazawa N, Park J H, Han J H, Matsui Y, Nagaosa N and Tokura Y 2010 *Nature* **465** 901

[3] Bogdanov A and Hubert A 1994 *J. Magn. Magn. Mater.* **138** 255

[4] Guslienko K 2008 *J. Nanosci. Nanotechnol.* **8** 2745

[5] Sampaio J, Cros V, Rohart S, Thiaville A and Fert A 2013 *Nature Nanotech.* **8** 839–844

[6] Soumyanarayanan A, Reyren N, Fert A and Panagopoulos C 2016 *Nature* **53** 509

[7] Uhlíř V, Urbánek M, Hladík L, Spousta J, Im M-Y, Fischer P, Eibagi N, Kan J J, Fullerton E E and Šikola T 2013 *Nature Nanotech.* **8** 341

[8] Lua S Y H *et al.* 2008 *Appl. Phys. Lett.* **93** 122504.

[9] Van Waeyenberge B, Puzic A, Stoll H, Chou K W, Tyliszczak T, Hertel R, Fähnle M, Brückl H, Rott K, Reiss G, Neudecker I, Weiss D, Back C H and Schütz G. 2006 *Nature* **444** 461

[10] Yamada K, Kasai S, Nakatani Y, Kobayashi K, Kohno H, Thiaville A and Ono T 2007 *Nature Mater.* **6** 270

[11] Fert A, Cros V and Sampaio J 2013 *Nature Nanotech.* **8** 153

[12] Peng R, Hu J, Yang T, Cheng X, Wang J, Huang H, Chen L and Nan C W 2018 *Mater. Res. Lett.* **6** 669

[13] Ghidini M, Mansell R, Pellicelli R, Pesquera D, Nair B, Moya X, Farokhipoor S, Maccherozzi F, Barnes C H W, Cowburn R P, Dhesi S S and Mathur N D, 2020 *Nanoscale*, DOI: 10.1039/C9NR08672B

[14] Li Q *et al.* 2017 *Appl. Phys. Lett.* **110** 262405

[15] Gilbert I *et al.* 2016 *Appl. Phys. Lett.* **109** 162404

[16] Schott M *et al.* 2017 *Nano Lett.* **17** 3006

[17] Nii, Y. *et al.* 2015 *Nat. Commun.* **6** 8539

[18] Schneider M *et al.* 2001 *Appl. Phys. Lett.* **79** 3113

[19] Bohlens S *et al.* 2008 *Appl. Phys. Lett.* **93** 142508

[20] Nakano K *et al.* 2011 *Appl. Phys. Lett.* **99** 262505

[21] Eerenstein W, Mathur N D and Scott J F 2006 *Nature* **442** 759

[22] Ghidini M, Maccherozzi F, Moya X, Phillips L C, Yan W, Soussi J, Métallier N, Vickers M E, Steinke N -J, Mansell R, Barnes C H W, Dhesi S S and Mathur N D 2015 *Adv. Mater.* **27** 1460

[23] Chopdekar R V *et al.* 2016 *Sci. Rep.* **6** 27501

[24] Gao Y *et al. Sci. Rep.* 2016 **6** 23696

[25] Li P *et al.* 2017 *ACS Appl. Mater. Interfaces* **9** 2642

[26] Lo Conte R *et al.* 2018 *Nano Lett.* **18** 1952

[27] Molegraaf H J A *et al.* 2009 *Adv. Mater.* **21** 1

[28] Skumryev V *et al.* 2011 *Phys. Rev. Lett.* **106** 057206

[29] Heron J T *et al.* 2014 *Nature* **516** 370

[30] Saenrang W *et al.* 2017 *Nature Commun.* **8** 1583

[31] Geprägs S *et al.* 2010 *Appl. Phys. Lett.* **96** 142509

[32] Wu T *et al.* 2011 *Appl. Phys. Lett.* **98** 012504

[33] Wu T *et al.* 2011 *Appl. Phys. Lett.* **98** 262504

[34] Sahoo S *et al.* 2007 *Phys. Rev. B* **76** 092108

[35] Lei N *et al.* 2013 *Nature Communications* **4** 1378

[36] Wang L *et al.* 2018 *Nature Mater.* **17** 1087

[37] Mitsuzuka K *et al.* 2016 *Appl. Phys. Lett.* **109** 162404

[38] Ostler T A *et al.* 2015 *Phys. Rev. Lett.* **115** 067202

[39] Wren T, Gribkov B, Petrashov V and Kazakova O 2015 *J. Appl. Phys.* **118** 023906

[40] Vansteenkiste A, Leliaert J, Dvornik M, Helsen M, Garcia-Sanchez F and Van Waeyenberge B 2014 *AIP Advances* **4** 107133

[41] Ghidini M, Zhu B, Mansell R, Pellicelli R, Lesaine A, Moya X, Crossley S, Nair B, Maccherozzi F, Barnes C H W, Cowburn R P, Dhesi S S and Mathur N D 2018 *J. Phys. D: Appl. Phys.* **51** 224007

[42] Thiaville A, Boileu F, Miltat J and Arnaud L 1988 *J. Appl. Phys.* **63** 3153

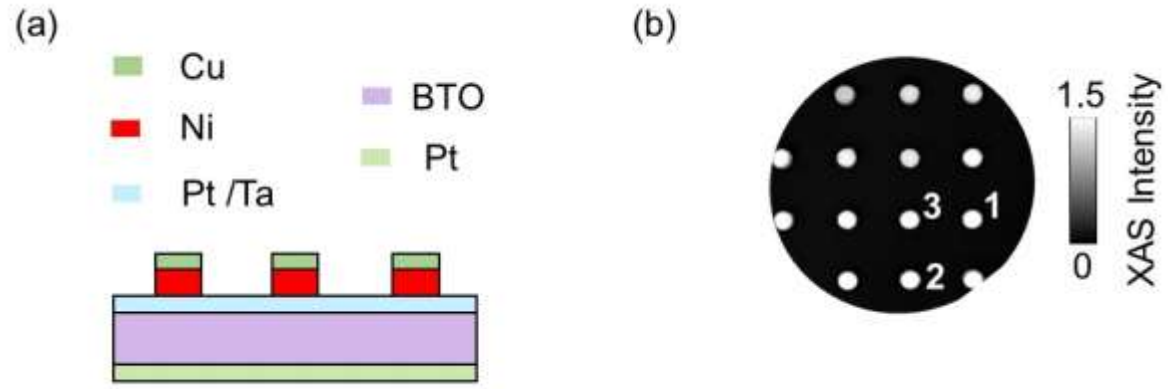

Fig. 1. Ni discs on BTO. (a) Cross-sectional schematic showing three of many Cu-capped Ni discs on an electroded BTO substrate in the pseudo-cubic (001) orientation. (b) XAS-PEEM image obtained in a 30 μm-diameter field of view. Discs 1-3 are numbered. Disc diameter 2 μm, Ni thickness 25 nm, Cu thickness 3 nm, top electrode is Pt(1.5 nm) on Ta(0.5 nm), bottom electrode is Pt (200 nm).

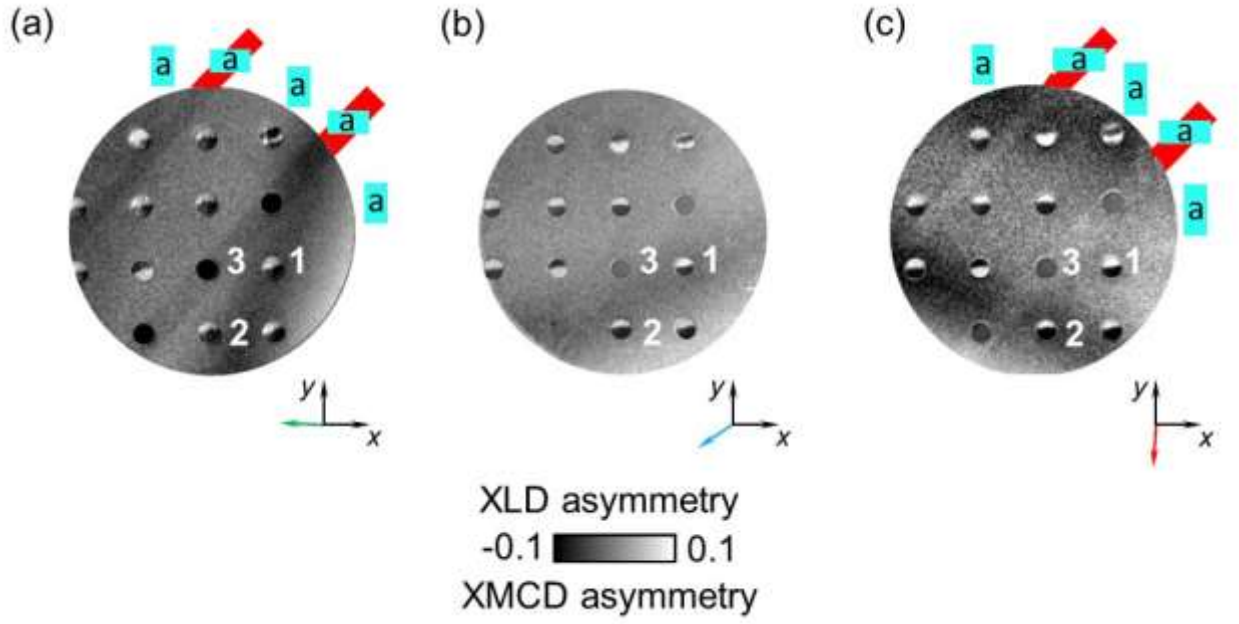

Fig. 2. Magnetic and ferroelectric imaging at 0 V. (a-c) Each panel shows an XMCD-PEEM image of Ni discs, and an XLD-PEEM image of the surrounding ferroelectric substrate. These images were obtained with the in-plane projection of the grazing-incidence X-ray beam parallel to the (a) green, (b) blue and (c) red arrow. Ferroelectric domains are resolved in (a) and (c), but not (b). BTO unit-cell schematics (light blue) represent the observed *a* domains. Red strips extrapolate the two *a* domains whose *c* axes lie parallel to *x*. The XMCD-PEEM and XLD-PEEM images were obtained in the same 30 μm-diameter field of view as the XAS-PEEM image in Fig. 1(b), and thus they include Discs 1-3.

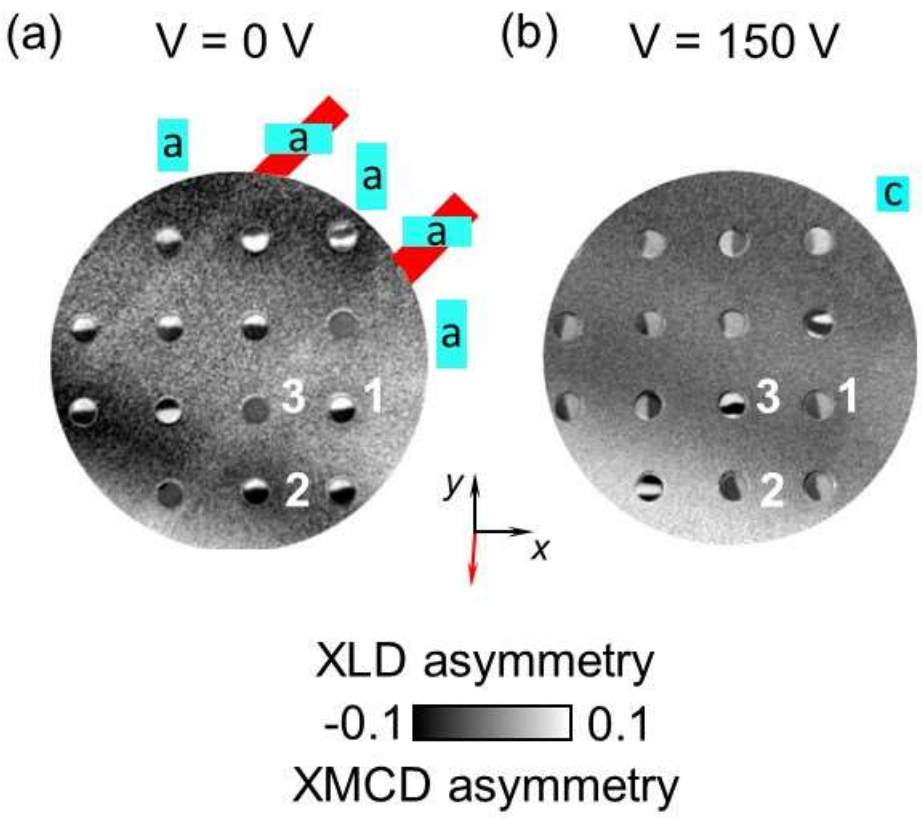

Fig. 3. Voltage-driven magnetoelectric switching. Panel (a) repeats the 0 V data of Fig. 2(c), for comparison with (b) the corresponding image at 150 V, where the BTO unit-cell schematic (light blue) represents the observed *c* domain.

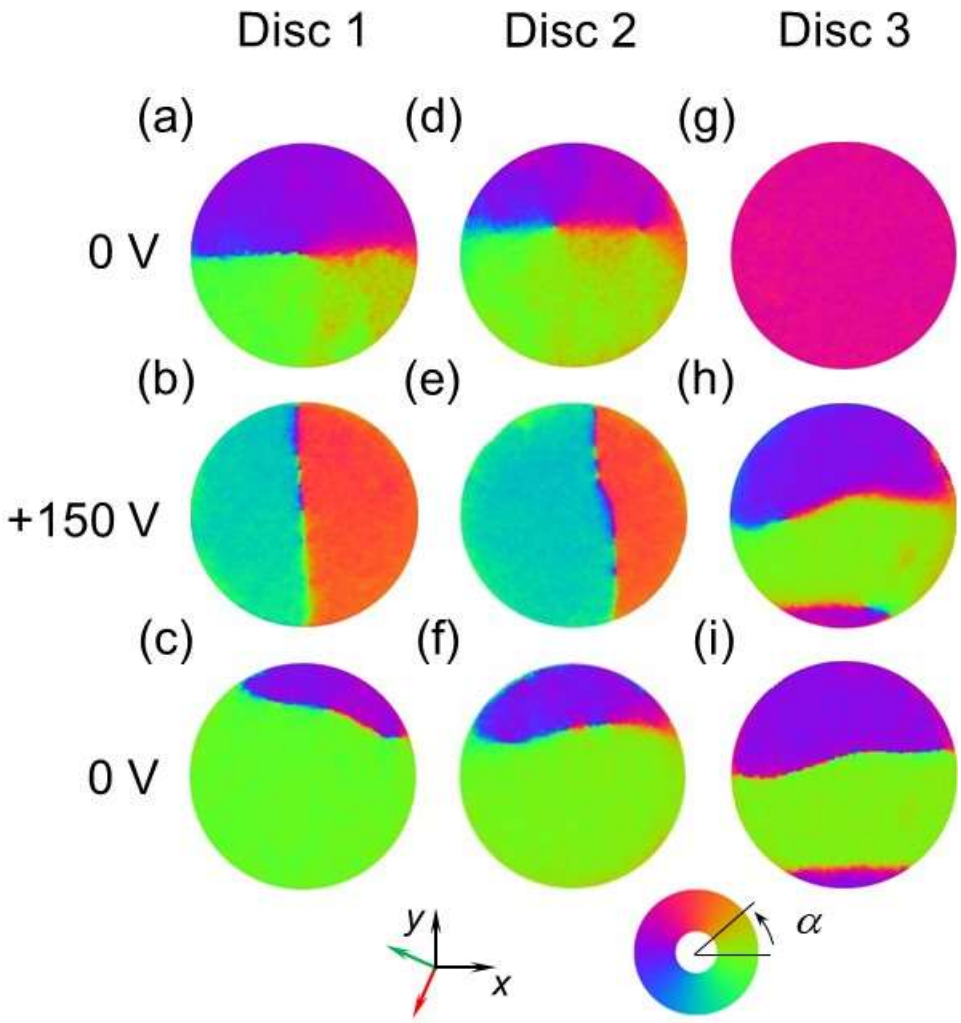

Fig. 4. Magnetic vector maps of discs 1-3 under voltage control. (a-i) Near-surface in-plane magnetization direction α for discs 1-3 when the voltage across the BTO substrate is cycled from 0 V to +150 V to -300 V (not shown) to 0 V. Each vector map represents the combination of two XMCD-PEEM images that were obtained in a 10 μm-diameter field of view with the in-plane projection of the grazing-incidence X-ray beam parallel to the red and green arrows. The unshown image for each disc at -300 V is similar to the corresponding image that we show for 150 V.

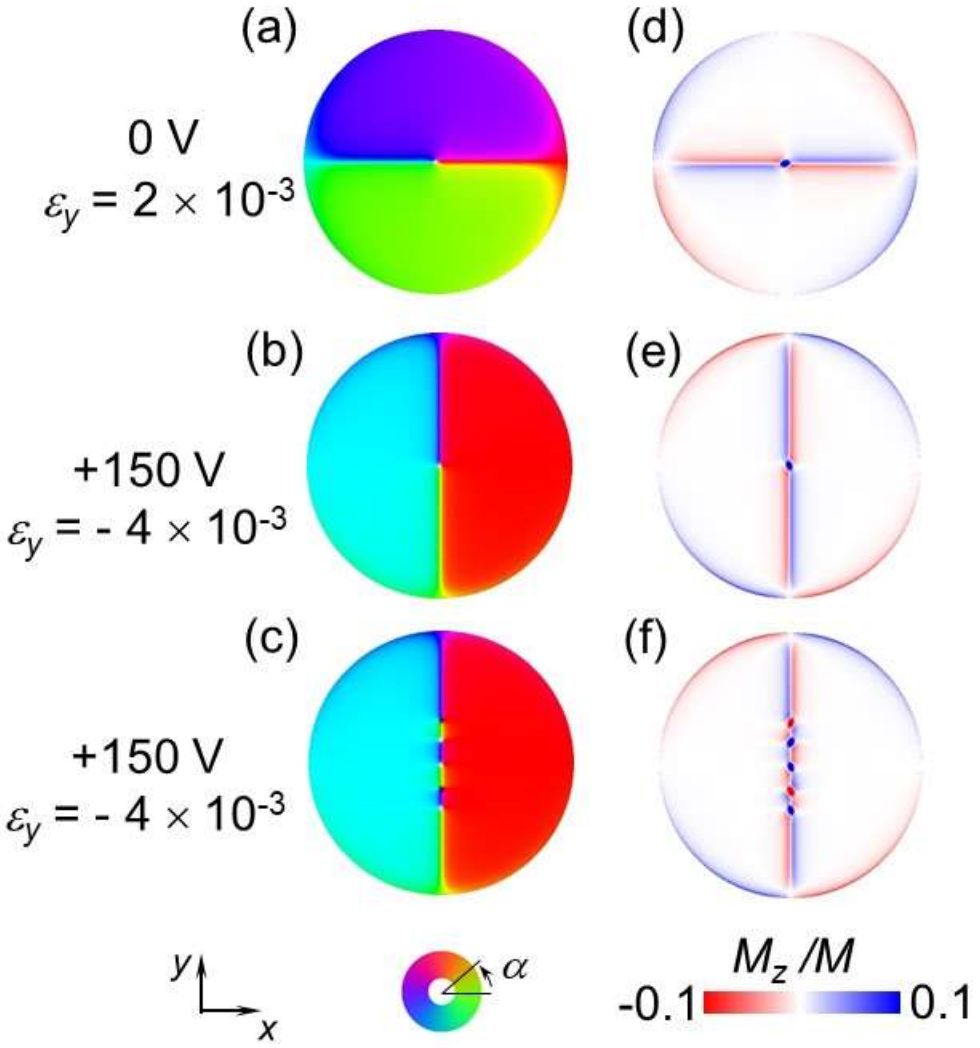

Fig. 5. Micromagnetic modelling of a Ni disc under strain-mediated voltage control. Maps of (a-c) in-plane magnetization direction α and (d-f) out-of-plane magnetization M_z describe the near-surface disc magnetization for the uniaxial strain ε_y that we identify with the application of (a,d) 0 V and (b,e) +150 V. Panels (c,f) assume the same strain as panels (b,e), and show a multivortex state whose energy is 0.2% higher. The magnitude of the local magnetization is denoted M.

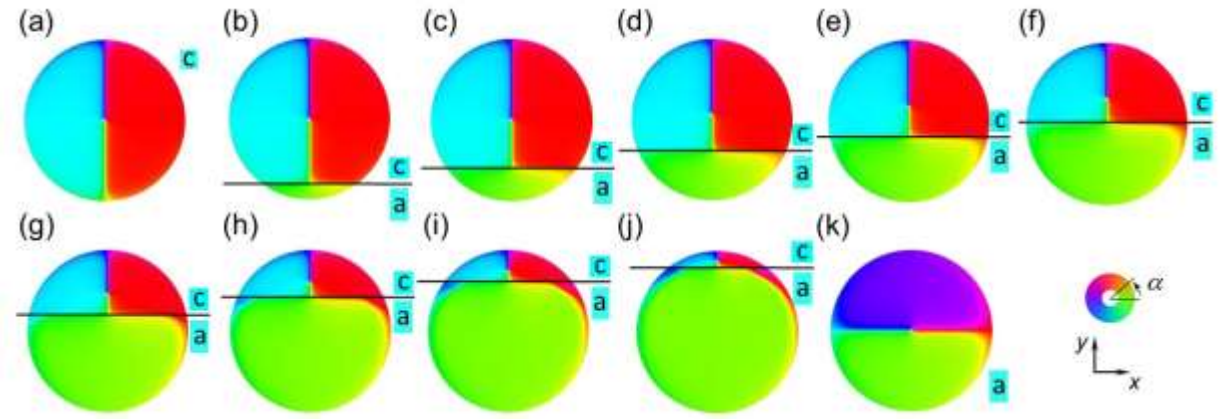

Fig. 6. Micromagnetic modelling of voltage-driven core displacement for a single vortex state. (a-k) Near-surface in-plane disc magnetization direction α during the transit of an *a*-*c* ferroelectric domain wall (black line), showing every other 100 nm step, such that the wall advances by 200 nm from one image to the next. The sequence corresponds to the removal of the experimentally applied +150 V, such that panel (a) matches the simulation in Fig. 5b, while panel (k) matches the simulation in Fig. 5a.

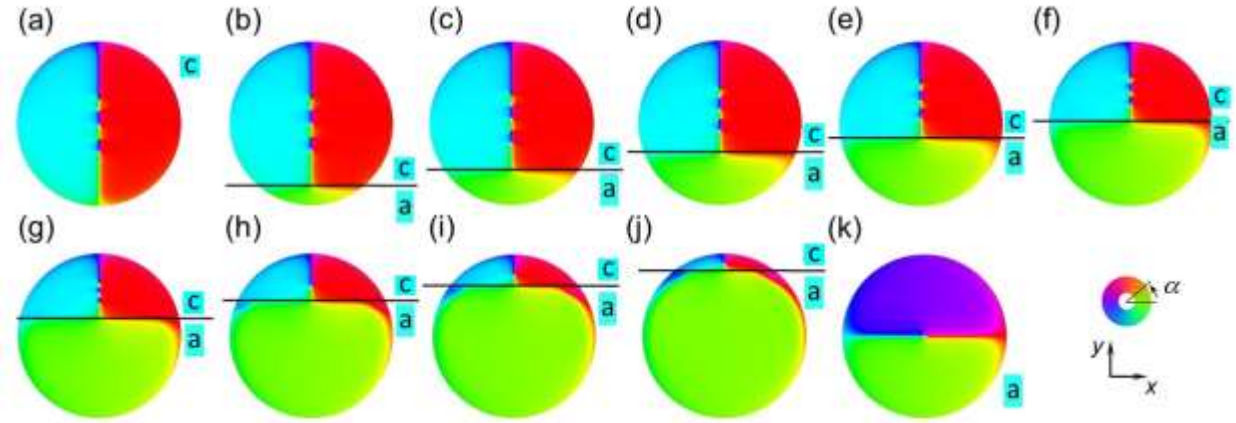

Fig. 7. Micromagnetic modelling of voltage-driven core displacements for a multivortex state. (a-k) Near-surface in-plane disc magnetization direction α during the transit of an *a*-*c* ferroelectric domain wall (black line), showing every other 100 nm step, such that the wall advances by 200 nm from one image to the next. The sequence corresponds to the removal of the experimentally applied +150 V, such that panel (a) matches the simulation in Fig. 5c, while panel (k) matches the simulation in Fig. 5a.